WVT-TR-76047

PRACTICAL FRACTURE MECHANICS APPLICATIONS TO DESIGN OF HIGH PRESSURE VESSELS

T. E. DAVIDSON
&
J. F. THROOP

DECEMBER 1976

BENET WEAPONS LABORATORY
WATERVLIET ARSENAL
WATERVLIET, N.Y. 12189

TECHNICAL REPORT

AMCMS No. 612105. H 84001

DA Project No. 1T162105AH84

Pron No. AW-7-R0003-01-AW-M7

DISCLAIMER

The findings in this report are not to be construed as an official Department of the Army position unless so designated by other authorized documents.

The use of trade name(s) and/or manufacturer(s) in this report does not constitute an official indorsement or approval.

DISPOSITION

Destroy this report when it is no longer needed. Do not return it to the originator.

SECURITY CLASSIFICATION OF THIS PAGE *(When Data Entered)*

REPORT DOCUMENTATION PAGE

READ INSTRUCTIONS BEFORE COMPLETING FORM

1. REPORT NUMBER: WVT-TR-76047	2. GOVT ACCESSION NO.
3. RECIPIENT'S CATALOG NUMBER	
4. TITLE *(and Subtitle)*: PRACTICAL FRACTURE MECHANICS APPLICATIONS TO DESIGN OF HIGH PRESSURE VESSELS	5. TYPE OF REPORT & PERIOD COVERED
	6. PERFORMING ORG. REPORT NUMBER
7. AUTHOR(s): Thomas E.Davidson and Joseph F. Throop	8. CONTRACT OR GRANT NUMBER(s)
9. PERFORMING ORGANIZATION NAME AND ADDRESS: Benet Weapons Laboratory Watervliet Arsenal, Watervliet, N.Y. 12189 SARWV -RT-TP	10. PROGRAM ELEMENT, PROJECT, TASK AREA & WORK UNIT NUMBERS: AMCMS Code; 612105. H8400; DA Proj No.1T162105AH84 PRON; AW-7-R0003-01-AW-M7
11. CONTROLLING OFFICE NAME AND ADDRESS: US Army Armament Command Rock Island, Illinois 61201	12. REPORT DATE: December 1976
	13. NUMBER OF PAGES: 45
14. MONITORING AGENCY NAME & ADDRESS *(if different from Controlling Office)*	15. SECURITY CLASS. *(of this report)*: UNCLASSIFIED
	15e. DECLASSIFICATION/DOWNGRADING SCHEDULE

16. DISTRIBUTION STATEMENT *(of this Report)*

Approved for public release; distribution unlimited.

17. DISTRIBUTION STATEMENT *(of the abstract entered in Block 20, if different from Report)*

18. SUPPLEMENTARY NOTES

19. KEY WORDS *(Continue on reverse side if necessary and identify by block number)*

Pressure Vessels Fracture Mechanics Fracture Toughness

Fatigue Cracks Stress Intensity Factor

20. ABSTRACT *(Continue on reverse side if necessary and identify by block number)*

Fracture Mechanics provides the rationale by which thick-walled pressure vessel designs may be assessed for adequacy of material toughness, for length of fatigue life, for necessary frequency of inspection and for fatigue life remaining after the detection of a given size crack.

Examples of the fatigue performance and fracture characteristics of thick-walled cylindersof high-strength steels are illustrated and (See Other Side)

DD FORM 1 JAN 73 1473 EDITION OF 1 NOV 65 IS OBSOLETE

SECURITY CLASSIFICATION OF THIS PAGE *(When Data Entered)*

20.
interpreted with pertinent fracture mechanics calculations. These provide insight for the designer into the various aspects of metallurgical control of strength and toughness, optimization of stress state through the use of residual stresses and importance of monitoring fatigue crack propagation.

TABLE OF CONTENTS

TABLES

LIST OF FIGURES

INTRODUCTION

The expanding use of high pressure technology is producing need for thick-walled pressure vessels that are capable of sustaining internal pressures of 5,000 to 100,000 psi or more. Such vessels are generally cylinders. As a matter of definition in this paper, a cylinder with a wall thickness greater than one-tenth of the internal diameter is considered to be thick walled. With a ratio of outside to inside diameter of 1.2 or more, this means that the stresses in the wall have a gradient that is properly expressed by the Lamé equations of elasticity theory.

The increasing use of such vessels, combined with increasing severity of service conditions, requires a critical re-examination of the philosophy of pressure vessel design in order to reduce the probability of unsatisfactory service life and/or catastrophic failures. The concept of designing for strength alone and using the highest strength material available without regard to toughness is likely to give dangerous results, since the attainment of high strength frequently results in low ductility and low fracture toughness. Low fracture toughness leads to fracture at small critical defect size, and under fatigue loading conditions the inherent defects in the material may be enlarged to this critical size quickly by sub-critical crack propagation. This results in short fatigue life and brittle fracture.

The nature of such behavior is illustrated by the results of tests of cannon tubes, which are essentially high-performance thick-walled cylinders. Figure 1 shows the fragments from a brittle fracture that

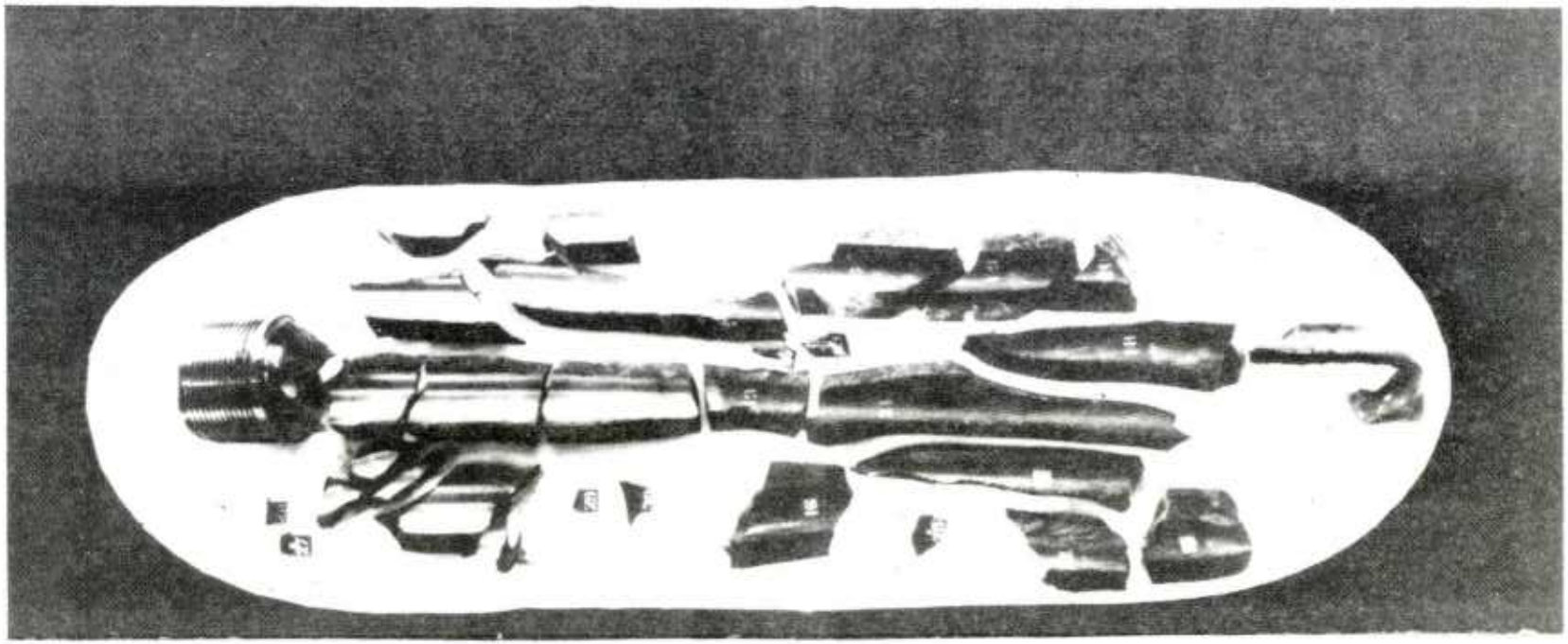

Figure 1. Fatigue Failure in Gun Tube. Fragments from brittle fracture produced by fatigue during firing tests of a developmental 175mm cannon tube.

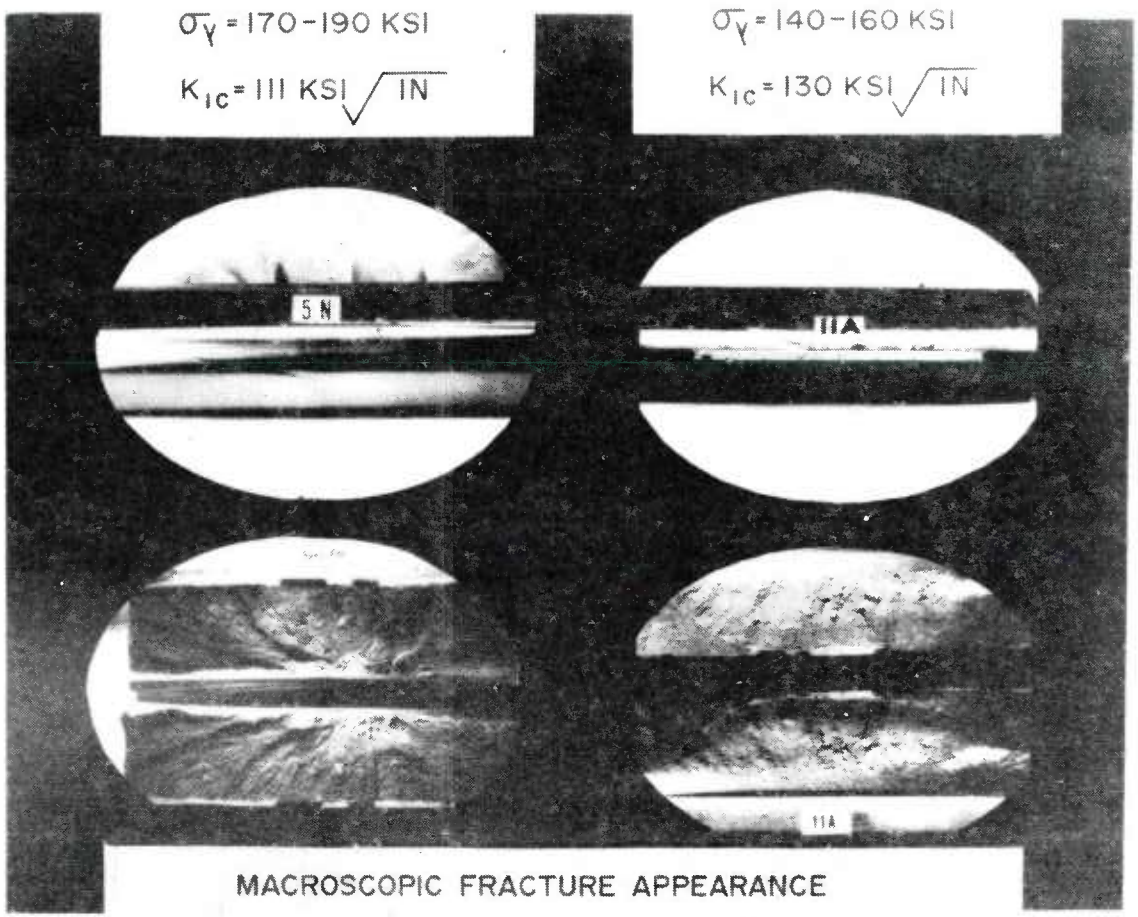

Figure 2. Macroscopic fracture appearance of fracture surfaces of cylinders with low and high fracture toughness showing the comparative critical crack depth at failure.

occurred during the test firing of a developmental 175mm cannon tube which had inadequate properties. Figure 2 shows fracture surfaces from laboratory fatigue tests of other 175mm tubes which were cycled at the firing pressure. These show the shallow critical crack depth corresponding to a fracture toughness of 111 ksi $\sqrt{in}$ and yield strength of 170-190 ksi, and the much greater critical depth for a fracture toughness of 130 ksi $\sqrt{in}$ and yield strength of 140-160 ksi in steel cylinders.

It is generally recognized that fatigue is a three stage process which involves initiation, stable crack propagation and, finally, unstable fast fracture. The latter two stages can be analyzed by fracture mechanics concepts. The portion of fatigue life endured during the initiation stage, however, must be considered at present as a bonus that depends upon favorable conditions. Crack initiation, being controlled by the shear strain range, is sensitive to yield strength. A high yield strength may provide a long initiation stage if the bore surface is smooth and undamaged in service, but any type of surface damage or stress discontinuity may cancel this advantage. When high strength metals are used the sensitivity to defects, surface conditions, environment and temperature makes the duration of the initiation stage difficult to estimate. Hence, in many applications, it may be best to neglect it and consider the fatigue life as that from some measureable size of flaw until failure.

The concepts of fracture mechanics provide a powerful tool which, when incorporated into the design process, directly addresses the questions of adequate strength and toughness, fatigue life expectancy,

necessary frequency of inspection and the fatigue life remaining after the detection of a fatigue crack of given size. They show that it is best to optimize the combination of yield strength and fracture toughness so that at the operating pressure the toughness is sufficient to sustain a critical crack depth approaching or equal to the wall thickness. This permits a "leak-before-fracture" with its attendant warning, making brittle fracture unlikely, and it also extends the fatigue crack propagation as far as possible.

Because the three-dimensional nature of the crack and stress configurations in thick cylinders presents severe difficulties in the analytical solution of crack problems, the practical application of fracture mechanics is limited at present to approximate solutions and to idealizations of experimentally measured behavior of cylinders. Such applications, even though approximate, may provide the designer with much insight into the roles of strength and toughness, the optimization of stress state by autofrettage or prestressing and the usefulness of monitoring of fatigue crack growth. The concepts, approximations and idealizations that may be applied will be illustrated with examples from fatigue tests of high strength steel cylinders.

FRACTURE MECHANICS

The basic fracture mechanics equations applicable to the problem are the Paris[1] equation for fatigue crack propagation rate

$$\frac{db}{dN} = \frac{1}{M}(\Delta K)^m \qquad (1)$$

1. Paris, P. C. "The Fracture Mechanics Approach to Fatigue", in Fatigue, an Interdisciplinary Approach, Burke, J. J., Reed, N. L. Weiss, V., Editors, Syracuse University Press (1964) pp 107-132.

and the expression for the stress intensity factor for the opening mode[2]:

$$K = Y S\sqrt{\pi b} \tag{2}$$

where, in the cylinder, b is the radial depth of the crack into the wall from the bore, N is the number of fatigue cycles, M is a material constant and the exponent m also depends upon the material. The ratio db/dN is the fatigue crack propagation rate at the deepest point of the crack. In cylinders pressurized from zero to maximum pressure, $\Delta K = (K_{max} - 0)$. Crack instability and fast fracture will occur when the stress intensity factor, from Equation 2, equals the fracture toughness K_{Ic} of the material. The relationship for the stress intensity factor is, then, basic to the problem of prediction of the fatigue and fracture of a pressurized cylinder.

In Equation 2 the value of S is that of the tangential bore stress given by the equation[3]

$$S = \left(\frac{w^2 + 1}{w^2 - 1}\right)p \tag{3}$$

where p is the internal pressure and w is the ratio of outside diameter to inside diameter. The term Y is a function of w and of the ratio (b/B) of crack depth b to the wall thickness B. It takes into account the variation of stress through the wall thickness. Stresses other than those caused by the pressure can be present, which will modify the stress intensity factor and, in turn, the crack growth rate. One important example is the residual stress state induced by autofrettage, jacketing, etc. These processes result in a compressive stress near the bore. This counteracts the tensile tangential stress expressed in Equation 3, resulting in a lower stress intensity factor

2. Paris, P. C. and Sih, G. C. "Stress Analysis of Cracks" in Fracture Toughness Testing and Its Applications ASTM-STP 381, Am. Soc. for Testing and Mats. (1965) pp 38-40.

for any given crack shape and a correspondingly lower crack growth rate.

An upper bound of stress intensity factors for wall cracks in cylinders is provided by the Bowie and Freese[4] solution for a straight fronted crack in a circular ring acted upon by an external traction T. In a tube this applies to a machined notch of depth b with its leading edge parallel to the axis of the tube. The tangential bore stress caused by an external traction T is[3]:

$$S = \left(\frac{2w^2}{w^2 - 1}\right) T \tag{4}$$

The Bowie and Freese expression for K_I is

$$K_I = H \left(\frac{1.12\ (2w^2)}{w^2 - 1} T \right) \sqrt{\pi b} \tag{5}$$

in which the Y of Equation 2 is seen to be 1.12 H. Values for H are given in Table I as a function of w and (b/B). For the diameter ratio w=2 the value of H is seen to be close to unity for b/B between 0 and 0.5.

For cylinders of diameter ratio w=2, if T=p the value of K expressed in terms of the internal pressure is

$$K_I = H\ (2.987)\ p \sqrt{\pi b} \tag{6}$$

This value of K is approximated for crack depths up to half the wall thickness by the expression

$$K = \left(1.12 \frac{w^2 + 1}{w^2 - 1} p + 1.13\ p\right) \sqrt{\pi b} \tag{7}$$

3. Timoshenko, S. and Goodier, J. N. "Theory of Elasticity", McGraw Hill Book Co., N. Y., Third Edition, p 71.

4. Bowie, O. L. and Freese, C. E., "Elastic Analysis for A Radial Crack in a Circular Ring", Engineering Fracture Mechanics, (1972) Vol. 4, pp 315-321.

TABLE I

THE NORMALIZED CORRECTION FACTOR, H
BOWIE AND FREESE, SINGLE CRACK

(b/B)	w = 1.25	w = 1.50	w = 1.75	W = 2.00	w = 2.25	w = 2.50
0.0	1.00	1.00	1.00	1.00	1.00	1.00
0.1	-	0.99	0.96	0.94	0.91	0.88
0.2	-	1.03	0.98	0.93	0.88	0.84
0.3	1.15	1.14	1.03	0.96	0.89	0.83
0.4	1.40	1.27	1.11	1.00	0.91	0.84
0.5	1.66	1.42	1.20	1.05	0.94	0.86
0.6	1.90	1.56	1.28	1.11	0.99	0.90
0.7	-	1.70	1.39	1.19	1.06	0.97
0.8	-	1.83	1.51	1.31	1.18	1.08
0.9	-	2.09	1.75	1.56	1.42	1.32

$$K = H \left[\frac{2.24\ w^2}{w^2 - 1} \right] T \sqrt{\pi b}$$

which gives $K = 3\ p\ \sqrt{\pi b}$ for cylinders of $w = 2$, as developed by Underwood et al[5] from the superposition of solutions for a side-notched plate under axial tension and pressure in the notch. The two terms within the bracket reveal the relative contributions to K for shallow cracks from the bore stress and the pressure in the crack. Their experimental strain and compliance data showed that this expression applied for a machined frontal notch in a 1-inch diameter steel cylinder. This is confirmed by the photoelastic measurements of C. W. Smith et al[6] using the stress freezing technique on similar notches in 1-inch diameter cylinders of this diameter ratio.

A graph of K/p for $w = 2$ from Equation 5 is shown as Curve (a) in Figure 3. Curve (b) is a plot of Equation 7 for the machined frontal notch. This corresponds to Equation 2 with a fixed value of $\alpha = 1.792$ for the term Y. The stress intensity factor for this frontal notch is so large that it exceeds the fracture toughness K_{Ic} of even the toughest steels at very shallow crack depths under usual operating pressures. Fortunately the natural crack growth does not maintain this shape, but tends to change toward a semi-elliptical shape which has a lower stress intensity factor. Otherwise many more brittle fractures of pressure vessels would have been experienced in service.

The values for K for curved fronted cracks are much smaller,

---

5. Underwood, J. H., Lasselle, R. R., Scanlon, R. D. and Hussain, M.A., "A Compliance K-Calibration for a Pressurized Thick-Wall Cylinder With A Radial Crack", Engineering Fracture Mechanics, (1972) Vol. 4, pp 231-244.
6. Smith, C. W., Jolles, M. and Hu, T., "Stress Intensities for Low Aspect Ratio Surface Flaws in Pressurized Thick Walled Tubes", Virginia Poly. Inst. Report VPI-E-75-19, Aug. 1975, Blacksburg, VA. 24061.

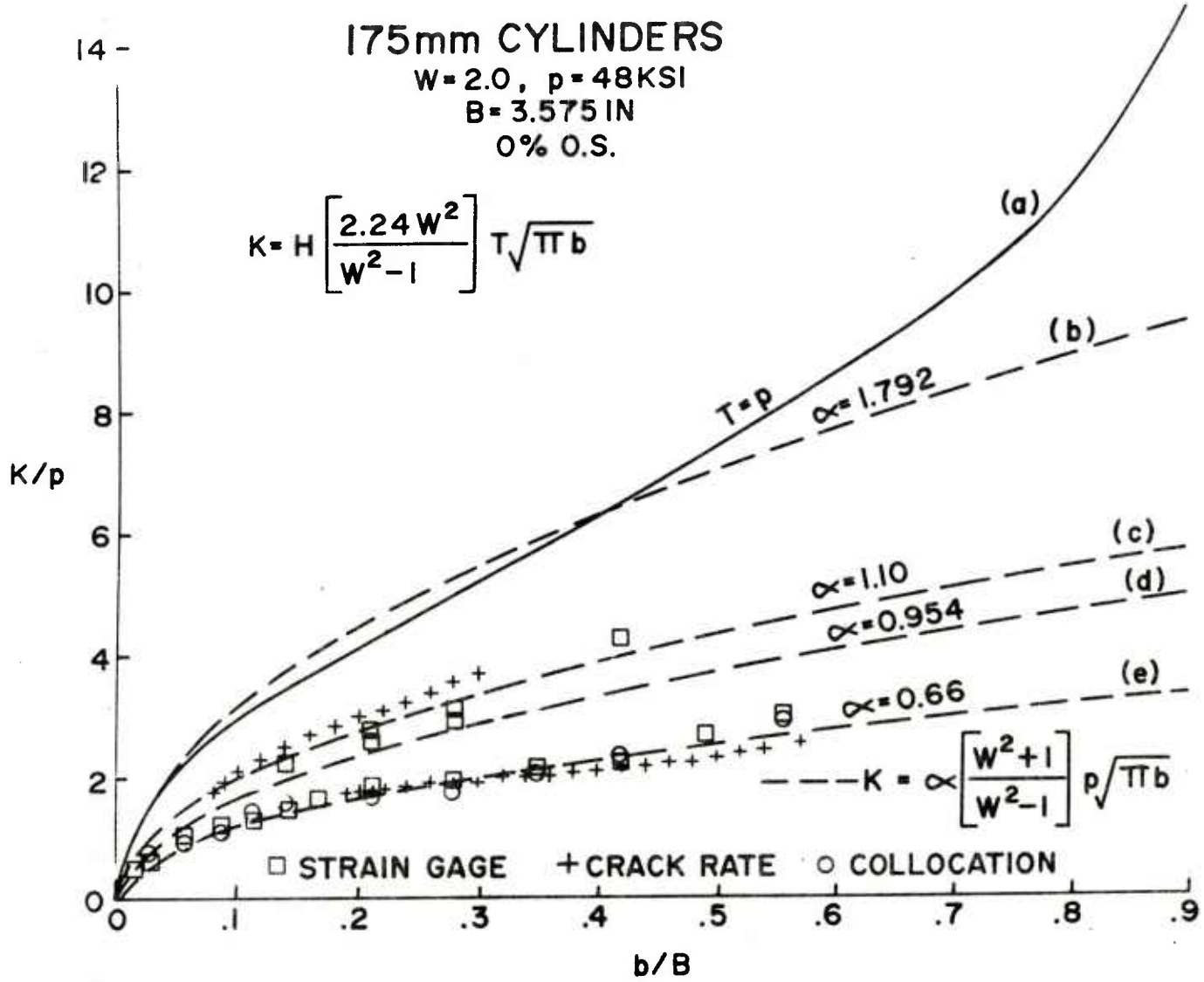

Figure 3. K/p versus b/B, 175mm cylinders. The graph shows the variation for a machined frontal notch, (a) and (b); a long curved crack, (c); a semi-elliptical crack, (d); and a semicircular crack, (e).

as illustrated by Curves (c), (d) and (e) in Fig. 3. These were obtained experimentally in 175mm cylinders of diameter ratio w = 2 from initial E.D.M. notches. The notches were 1/4 inch deep in a wall thickness of 3.575 inches. The stress intensity factors decrease with increasing curvature of the crack front. Curve (c) with $\alpha = 1.10$ is for a long curved crack grown from a 20-inch long notch. Curve (d) with $\alpha = 0.954$ is for a semi-elliptical crack grown from a 4-inch long notch and Curve (e) with $\alpha = 0.66$ is for a semicircular crack grown from a 1/2-inch notch. The latter is confirmed to a depth of one-half the wall thickness by the results of collocation analysis by Hussain[7] et al, as indicated by the circles on the graph. This lower curve represents the lower bound of K for wall cracks in non-autofrettaged cylinders of w = 2 diameter ratio.

Experimental data from compliance measurements are represented by squares on Fig. 3. Data from crack rate comparison with a C-shape specimen of known K-calibration and of the same material are shown by crosses. The curves and data are in agreement for crack depths up to 4/10 of the wall thickness. Since over 80% of the fatigue life is endured before this depth is reached the integration of Equation 1 using the constant values of α for Y in Equation 2 appears to be reasonable.

---

7. Hussain, M. A., Pu, S. L., Scanlon, R. D., and Throop, J. F., "Stress Intensity Factor for A Pressurized Thick-wall Cylinder with Part Through Circular Flaw, Collocation Method and Compliance Calibration", in preparation, (1976).

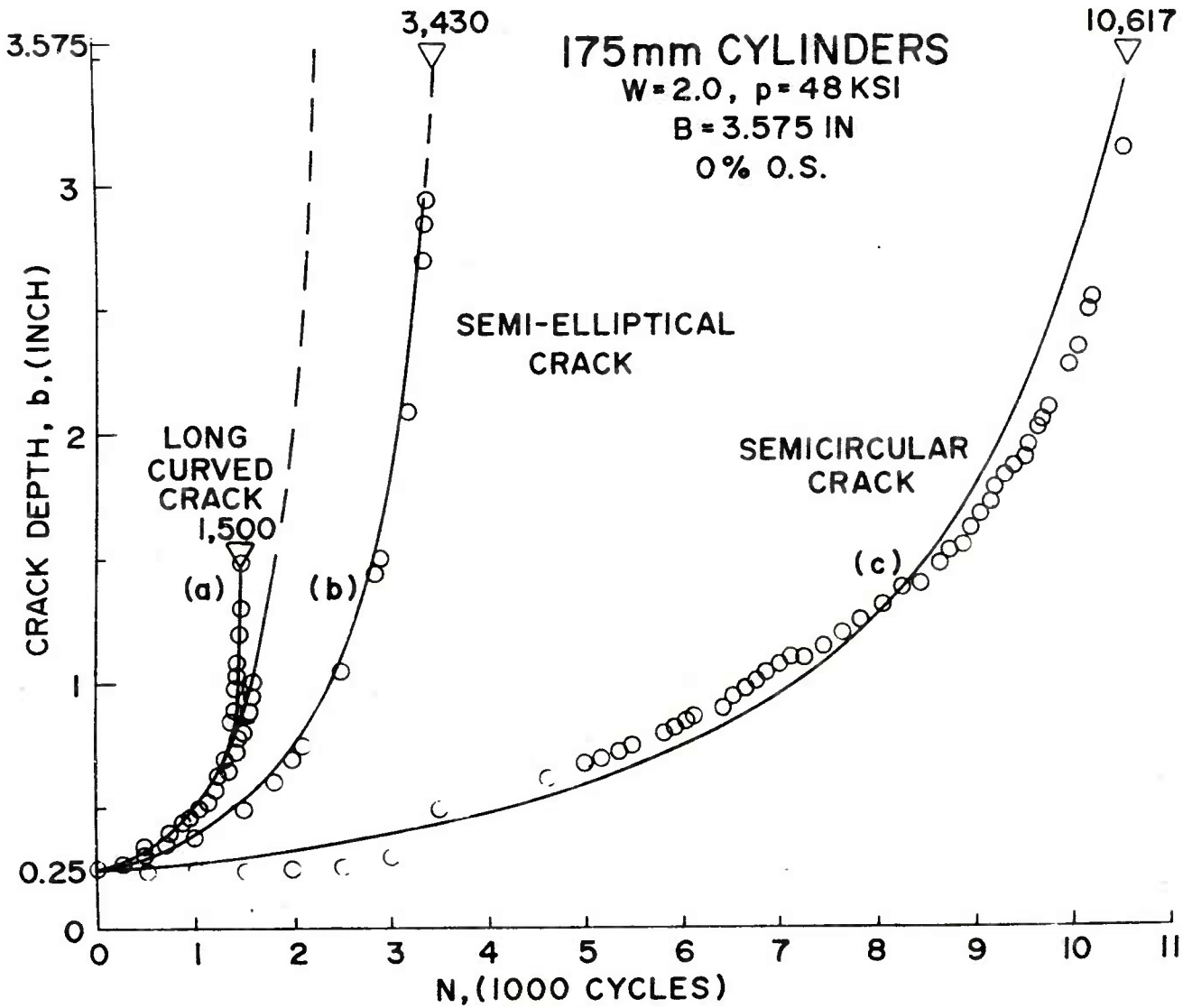

Figure 4. Crack depths versus N, cycles, in 175mm cylinders. The graph shows fatigue crack propagation curves for three crack shapes in cylinders of 2.0 diameter ratio under cyclic pressurization to 48 ksi, showing data and calculated curves.

FATIGUE CRACK GROWTH

Expressing K by using a constant α for the term Y in Equation 2, as plotted in Fig. 3, permits the simple integration of Equation 1 in the form

$$\int_{Ni}^{N_b} dN = M \int_{b_i}^{b} (\Delta K)^{-m} \, db \qquad (8)$$

This gives the expression for remaining fatigue crack propagation life, $(N_f - N_i)$, from a crack depth b_i to any final crack depth b_f at a given cyclic pressure as:

$$(N_f - N_{i)} = M \; \pi^{\frac{-m}{2}} \; (\alpha \, S)^{-m} \int_{b_i}^{b_f} b^{-m/2} \, db \qquad (9)$$

Analysis of the fatigue crack growth monitored by ultrasonics during tests of 175mm cylinder specimens indicates that the integer exponent which represents the data most satisfactorily is m = 3.

With the value m = 3 the remaining crack life becomes

$$(N_f - N_i) = 2M\pi^{-3/2} \left(\alpha \frac{w^2+1}{w^2-1} \, p\right)^{-3} \left[\frac{1}{\sqrt{b_i}} - \frac{1}{\sqrt{b_f}} \right] \qquad (10)$$

This shows a strong influence of crack shape on fatigue life because it is expressed by α raised to the power of three. This influence is illustrated in Figure 4 with plots of crack depth versus cycles for (a) the long curved crack, (b) the semi-elliptical crack and (c) the semicircular crack. The data points shown are from crack depths measured by ultrasonic techniques during the fatigue tests of 175mm cylinder cycled at 48 ksi internal pressure. The crack sizes were monitored from an initial depth of 1/4-inch until failure.

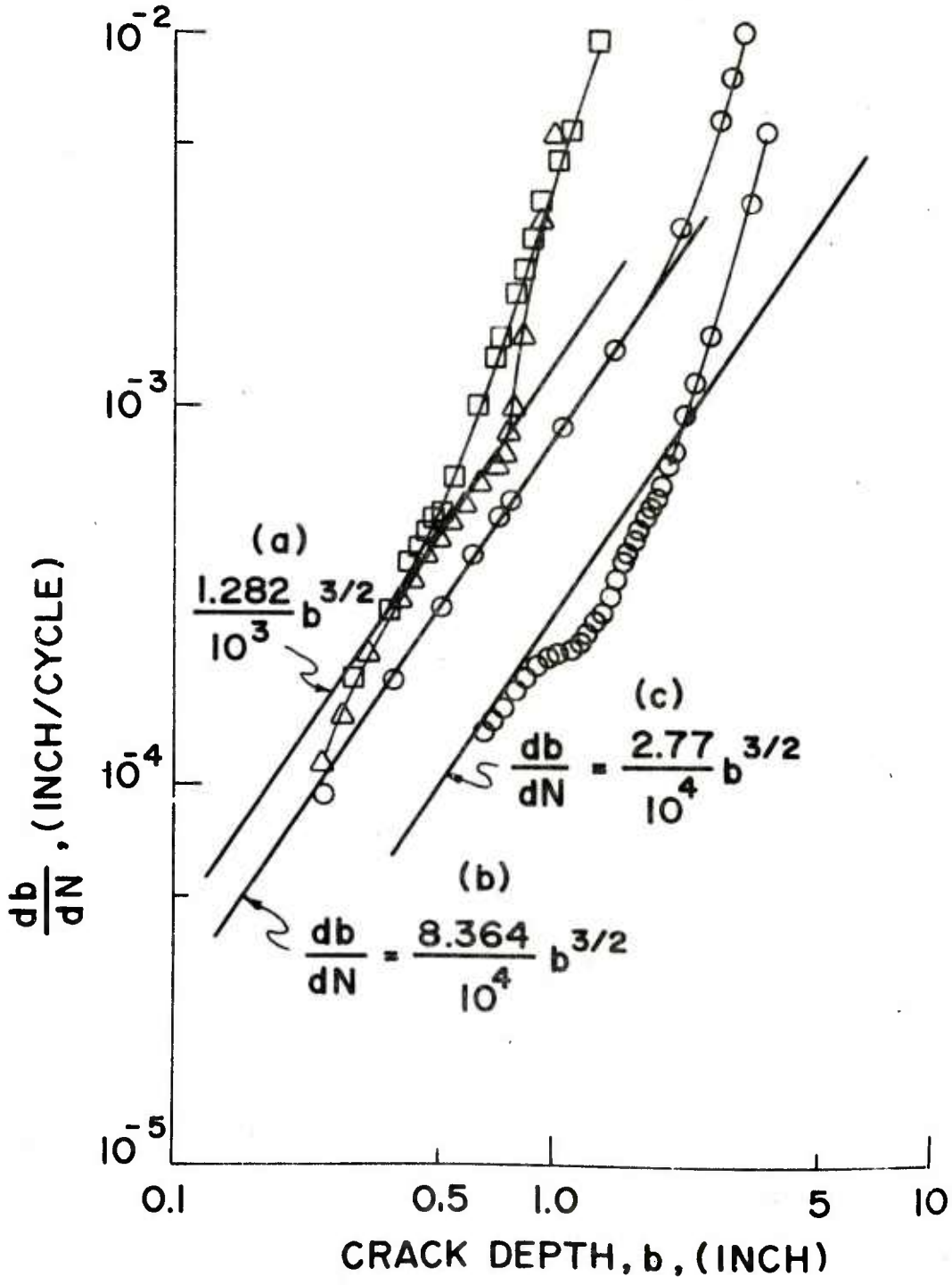

Figure 5. Crack rate versus crack depth, 175mm cylinders. The log-log graph shows the fatigue crack propagation rate for three crack shapes, showing data and calculated lines

The smooth curves on the graph were calculated from Equation 10, using the idealized expressions

$$\frac{db}{dN} = 3.379 \times 10^{-10} (\Delta K)^3 \qquad (11)$$

and

$$K = \alpha\left(\frac{w^2 + 1}{w^2 - 1}\right) p \sqrt{\pi b} \qquad (12)$$

with α = 1.10, 0.954 and 0.66 for the three shapes, respectively. Thus, with these values of α, and with M = 2.959×10^9, w = 2, p = 48, and b_i = 0.25 in Equation 10, the calculated curves approximate the measured crack growth data reasonably well from the 1/4-inch initial crack depth to failure. The fatigue lives for the three crack shapes were 1,500, 3,430 and 10,617 cycles respectively.

Figure 5 shows the corresponding crack propagation rates on a log-log plot of db/dN versus b. The data points show the crack rates obtained from the measured depth - cycles data. The idealization of these rates are shown by the straight lines on the graph, calculated using the coefficient

$$\frac{1}{M} = \frac{C}{(E\, S_Y\, K_{I_C})} \qquad (13)$$

in Equation 1, as proposed by Throop and Miller[9] to relate the fatigue crack rate to the mechanical properties in tempered martensitic steels. With the exponent m = 3 and the material properties listed in Table II for these cylinders, Equation 11 corresponds to the expression

9. Throop, J. F. and Miller, G. A., "Optimum Fatigue Crack Resistance", in "Achievement of High Fatigue Resistance in Metals and Alloys", ASTM-STP 467, Am Soc. for Testing and Mats. (1970), pp 154-168.

TABLE II

REPRESENTATIVE COMPOSITION, PROPERTIES, AND CRACK RATES

C	0.34
Mn	0.50
P	0.012
S	0.011
Si	0.22
Ni	3.08
Cr	1.15
Mo	0.58
V	0.13

E	=	3×10^4	KSI
S_u	=	190	KSI
S_Y	=	170	KSI
ELONG	=	18	%
RA	=	50	%
υ	=	0.3	POISSON'S RATIO
C_V	=	25	FT.LB. (-40°F)
K_{Ic}	=	140	KSI(IN)1/2
R_c	=	40	ROCKWELL HARDNESS

$da/dN = 1.51 \times 10^{-8} (\Delta K)^2$

FOR $K < 94$ KSI$(IN)^{1/2}$

After Barsom[8]

$da/dN = 4.5 \times 10^{-12} (\Delta K)^4$

FOR $K > 94$ KSI$(IN)^{1/2}$

After Throop and Miller[9]

$$\frac{db}{dN} = 3.379 \times 10^{-10} (\Delta K)^3$$

$20 < K < 200$ KSI$(IN)^{1/2}$

$$\frac{db}{dN} = \frac{0.24}{(E\ S_y\ K_{Ic})}\ (\Delta K)^3 \qquad (14)$$

and results in the lines of constant slope on Fig. 5. Since ΔK is a function of the square root of the crack depth b and the crack rate is proportional to $(\Delta K)^3$, the idealized crack propagation rate is a function of $b^{3/2}$ as represented by these lines. Other crack rate relationships for high strength steels, dependent on $(\Delta K)^2$ as suggested by Barsom[8] and on $(\Delta K)^4$ as proposed by Throop and Miller[9] did not approximate this data as well when used with ΔK as expressed in Equation 12.

Figure 5 shows that, although the measured crack propagation rates are not matched exactly, approximating them in the range between 10^{-4} and 10^{-3} inch/cycle is sufficient to approximate the depth versus cycles data shown on Fig. 4. Closer approximation will require the use of variable coefficients and exponents and recourse to numerical integration. This will require more precise knowledge of the effects of material properties, crack shape changes, stress gradients, etc. on the crack propagation rate.

CRITICAL DEPTH

The critical crack depth can be estimated by the expression

$$b_c = \frac{1}{\pi}\left(\frac{K_{Ic}}{\alpha\ S}\right)^2 \qquad (15)$$

8. Barsom, J. M., "The Dependence of Fatigue Crack Propagation on Strain Energy Release Rate and Crack Opening Displacement", in Damage Tolerance in Aircraft Structures", ASTM-STP 486, Am. Soc. for Testing and Mats. (1971) pp 1-15.
9. Throop, J. F. and Miller, G. A., "Optimum Fatigue Crack Resistance", in "Achievement of High Fatigue Resistance in Metals and Alloys", ASTM-STP 467, Am Soc. for Testing and Mats. (1970), pp 154-168.

TABLE III

CRACK SHAPES AND FAILURE CONDITIONS

Cylinder No.	Initial Notch	Crack Shape	α	S ksi	b_c (inch)	b_f (in)	$\left(\frac{b_f}{b_c}\right)$	K_{If} (ksi $\sqrt{in}$	$\left(\frac{K_F}{K_{IC}}\right)$
AM2448B	20"	Long curved	1.10	100	0.516	1.0	1.94	195	1.39
AM2437B	20"	Long curved	1.10	80	0.806	1.5	1.86	191	1.36
CM2437B	4"	Semi-ellipse	0.954	80	1.071	2.95	2.75	232	1.66
B2448B	1/2"	Semicircle	0.660	80	2.238	3.575	1.60	176	1.26

Note: $K_{IC} = 140$ Ksi $\sqrt{in}$; $b_c = \frac{1}{\pi}\left(\frac{K_{IC}}{\alpha S}\right)^2$; $K_{If} = \alpha \; S \; \sqrt{\pi b_f}$

Our experimental results indicate that for curved crack shapes in non-autofrettaged cylinders this is a conservative estimate. The depths, b_f, at fatigue failure shown in Table III are at least 60% larger than b_c calculated using K_{Ic} = 140 ksi for this material. This corresponds to a value of $K_{If} = \alpha S\sqrt{\pi b_f}$ at fatigue failure which is at least 1.26 K_{Ic}. The measured K_{Ic} value was obtained using a C-shaped specimen of known K-calibration taken from one of the cylinders. It appears that because the rest of the curved crack front is at lesser K than the deepest point the fracture may be delayed by triaxial constraint even though the crack rate at the deepest point is related to the value of ΔK at that point.

CRACK SHAPE

The Bowie and Freese solution for K of the frontal notch takes into account the effect of size, stress gradient and diameter ratio through the quantities H and w. A useful empericism, as yet unverified, is to assume that the K for other crack shapes may be found by taking a fraction of the K for the frontal crack. This is equivalent to using a reduced traction T in Equation 5; for instance T = 0.39 p for the semicircle, T = 0.52 p for the semi-ellipse and T = 0.625 p for the long curved crack. The latter value corresponds to the external traction T that, acting alone with w = 2, would produce the same tangential bore stress as would the internal pressure acting alone, since this requires that $T = \left(\frac{w^2 + 1}{2w^2}\right) p = \frac{5}{8} p$. Curves for these reduced equivalent values of T are shown in Figure 6 along with the curves previously shown in Figure 3. Curves (f), (g)

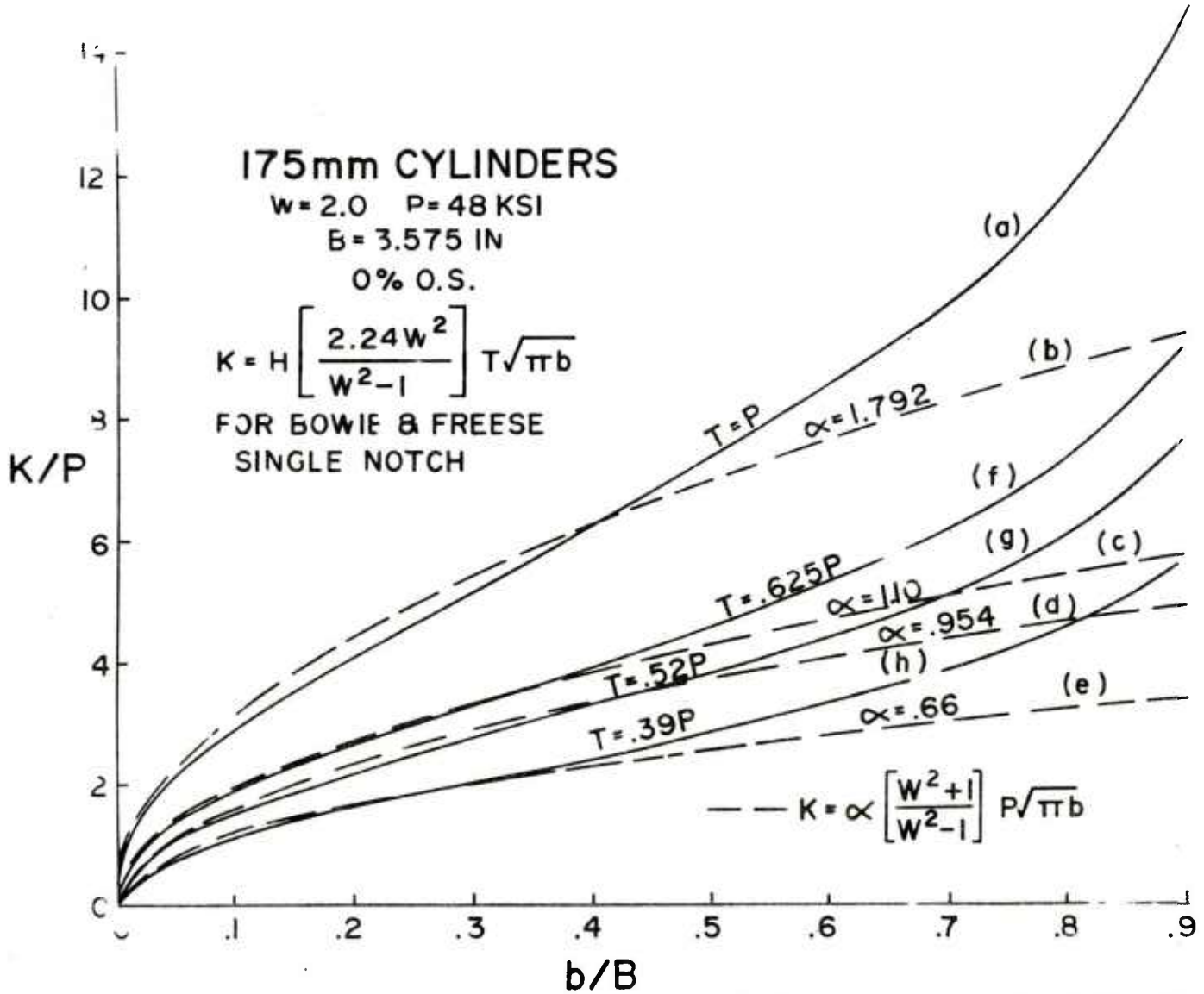

Figure 6. K/p versus b/B at fractional traction. The graph shows curves calculated from the Bowie and Freese solution by use of a "reduced traction" corresponding to each crack shape in 175mm cylinders of 2.0 diameter ratio.

and (h) are for the long curved crack, the semi-elliptical crack and the semicircular crack respectively. The use of appropriate "reduced tractions" for similar crack shapes in tubes of other bore sizes and wall ratios is yet to be experimentally evaluated.

In Fig. 6 Curves (a), (f), (g) and (h) represent the K for cracks of constant crack shape, whereas curves (c), (d) and (e) represent K for cracks that are changing shape as they deepen by fatigue. It is apparent that the latter cut across curves of lower and lower K as the crack grows. The changes in crack shape from the three initial notches are shown in Figures 7, 8 and 9.

SIMILITUDE

For wall cracks in cylinders where $K = \alpha S \sqrt{\pi b}$ is a reasonable approximation for the stress intensity factor and which have sufficient toughness to sustain a "leak-before-fracture", the failure crack depth, b_f, can be taken as the wall thickness B, and Equation 10 can be written as:

$$(N_f - N_i) = \mathfrak{D} \left[\sqrt{\frac{B}{b}} - 1 \right] \tag{16}$$

where

$$\mathfrak{D} = \left[2 \pi^{-3/2} M \alpha^{-3} \left(\frac{w^2 + 1}{w^2 - 1} p \right)^{-3} \frac{1}{\sqrt{B}} \right] \tag{17}$$

Thus, two cylinders will have the same fatigue crack propagation lives for the same ratio of initial crack depth to wall thickness, (b_i/B), if their values of $\mathfrak{D}$ are equal. If they are unequal, the one with the larger value of $\mathfrak{D}$ will have the longer life.

The constant M depends on the choice of material. The quantities

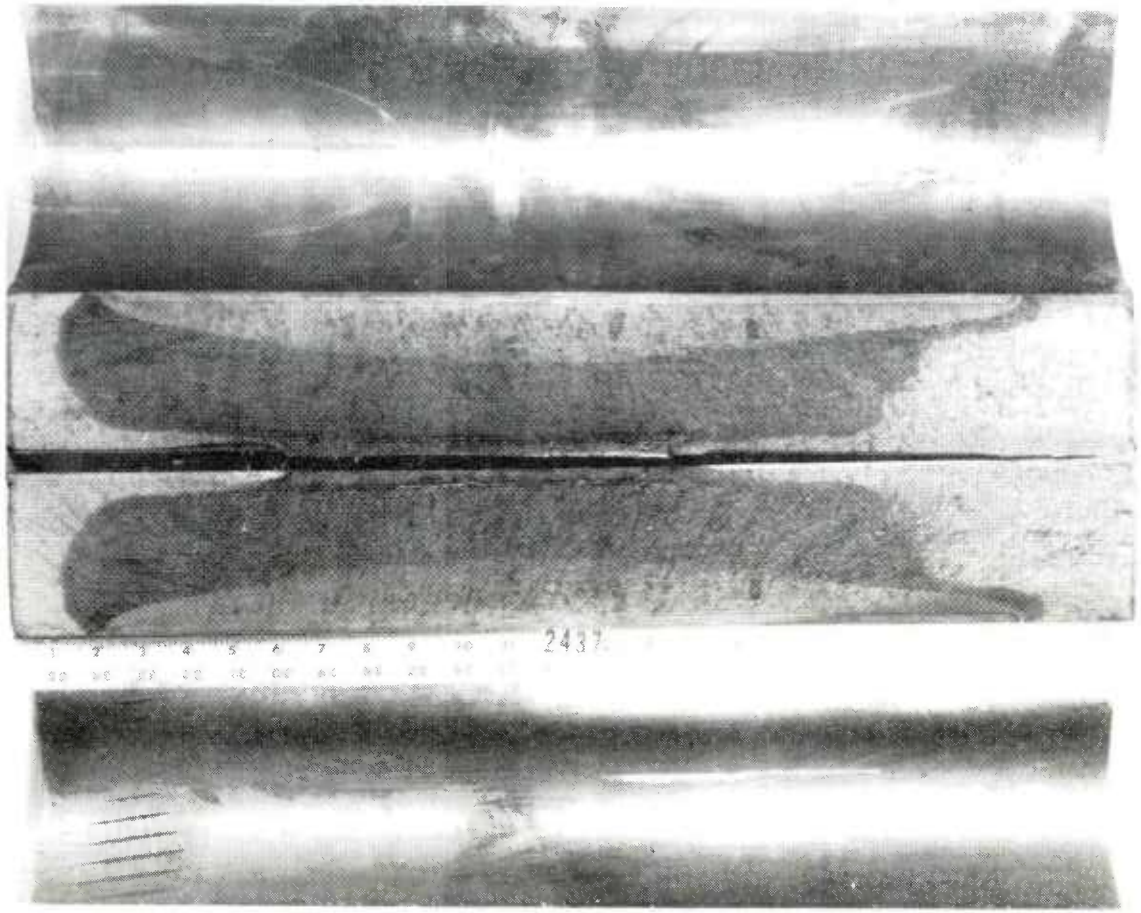

Figure 7. Fracture surface, long curved crack. The photo shows the 20-inch long notch, 1/4 inch deep in 175mm cylinder AM2437B and shows the long curved crack developed by fatigue to N = 1,500 cycles and failure from 1.5 inch crack depth.

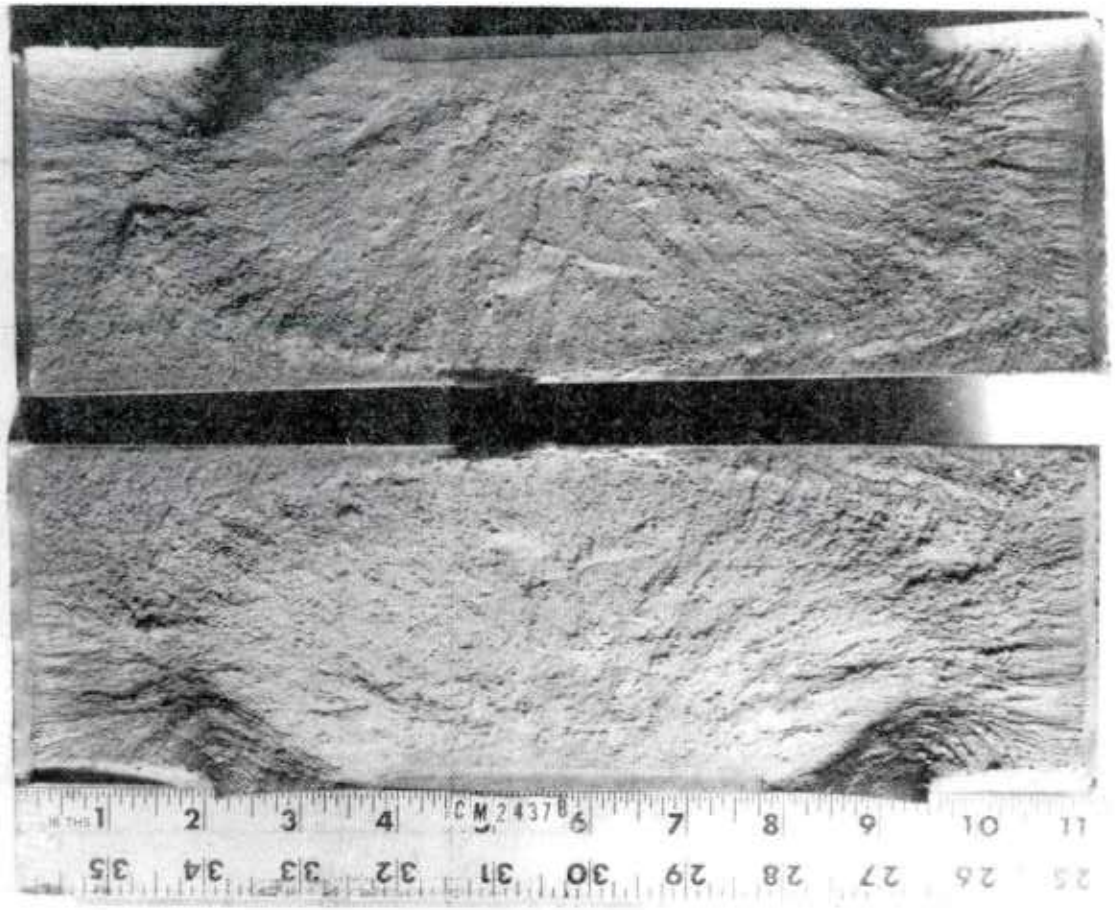

Figure 8. Fracture surface, semi-elliptical crack. The photo shows the 4-inch notch,]/4 inch deep in 175mm cylinder CM2437B and shows the semi-elliptical crack shape developed by fatigue to N = 3,430 cycles and failure through the 3.575 inch thick wall.

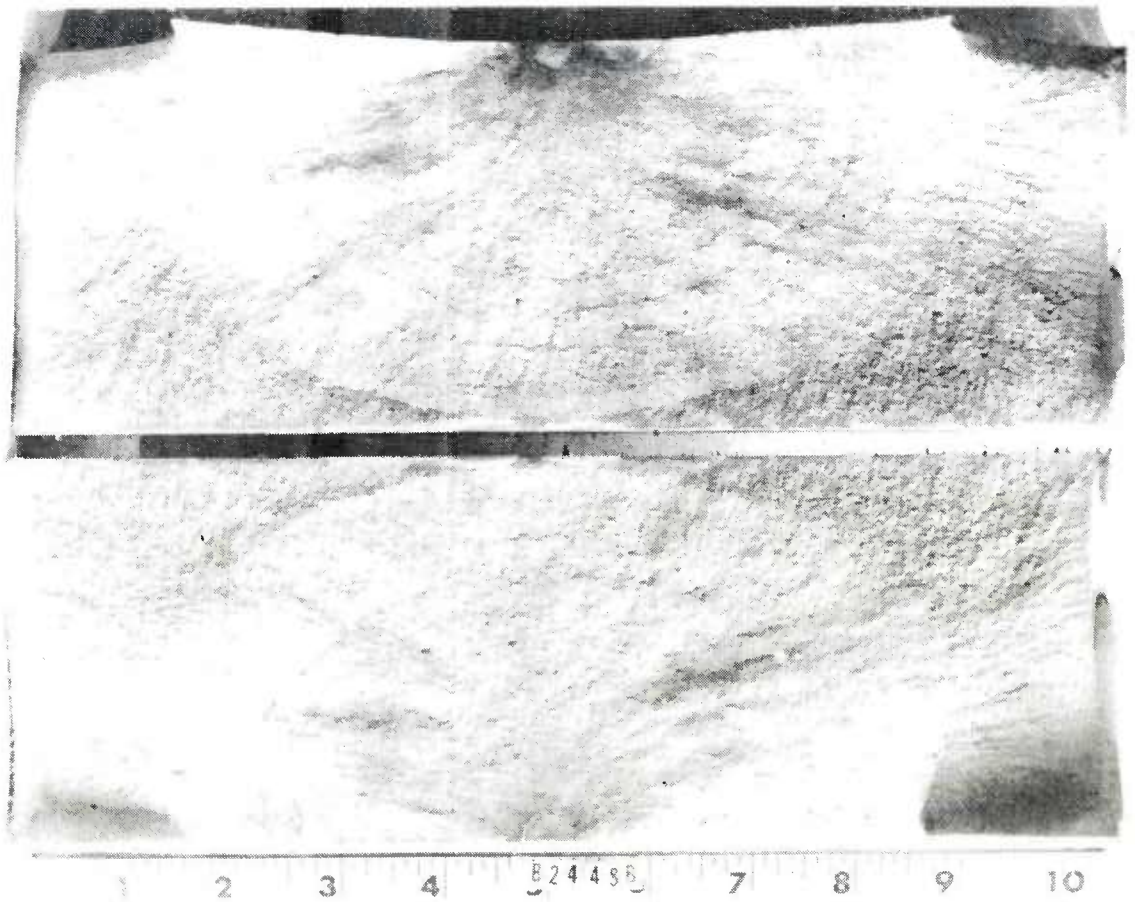

Figure 9. Fracture surface, semicircular crack. The photo shows the]/4 inch radius initial notch and the semicircular crack growth which finally became elliptical by N = 10,617 cycles and fatigue failure through the 3.575 inch thick wall.

p, w and B can be adjusted by design geometry, while the value of α for a given crack shape can be changed by autofrettage or prestressing to produce residual compressive stress at the bore. The quantity $\mathfrak{D}$, then, expresses the effect of these design variables upon the remaining fatigue life $(N_f - N_i)$.

PRACTICAL APPLICATION

Since the remaining fatigue life $(N_f - N_i)$ is linearly proportional to the value of $\mathfrak{D}$, this quantity enables the comparison of lives of different cylinder designs, with different sizes, operating pressures and amounts of overstrain on a basis which accounts for the differences.

The major difficulty in establishing the proper value of $\mathfrak{D}$ lies in the evaluation of α, the remainder of the variables being materials and configuration characteristics which can be selected. In the absence of residual stresses the value of α depends upon the crack shape and ranges from 1.792 for the frontal notch to 0.66 for the semicircular crack. Thus one is faced with a wide range of choice, for which some general guidance can be given. If in the application there are no discontinuities occurring along the bore, so that crack initiation can be more or less random, and if toughness is sufficient to sustain considerable crack depth, one can safely assume that the crack of concern will be of semi-elliptical or semicircular shape. Thus the value of will be between 0.945 and 0.66. Use of the higher value is the more conservative estimate. If toughness is low or if a continuous longitudinal discontinuity exists or may be introduced in operation, one must assume that a long crack will form and values of α from 1.792

to 1.10 should be chosen. It is likely that the lower value (1.10) will safely apply to the majority of cases of this type, except where K_{Ic} is very low.

As stated previously, residual stresses will modify the value of the stress intensity factor for a given crack shape. Autofrettage overstrain produces compressive residual stresses at the bore and alters the stress distribution through the wall considerably. This serves to reduce α in the stress intensity factor expression, particularly at shallow crack depths. As the crack deepens into the region of tensile residual stress the stress intensity factor may continue to be expressed in terms of the reduced α, presumably because of the gradual relaxation and equilibration of the residual stresses near the advancing crack front. Although quantitative definition of the effects of autofrettage and residual stresses on α is the subject of current study, some insight into the effect can be obtained from examining the values of α associated with some cases of observed and measured crack growth in autofrettaged cylinders. Moreover, this will serve to demonstrate the important role that residual stresses can play in enhancing fatigue behavior.

One example is a sample of four 175mm tubes[10] which were partially overstrained (40% of the wall thickness) by hydraulic autofrettage and fatigue tested to failure. The graphs of crack depth versus cycles, measured with ultrasonics, are shown on Figure 10 along with a

---

10. Davidson, T. E., Reiner, A. N. Brown, B. B., Throop, J. F., Miller, J. J. and Austin, B. A., "The Fatigue Life Characteristics of the 175mm M113E1 Gun Tube", Watervliet Arsenal Technical Report WVT-6912, March 1969.

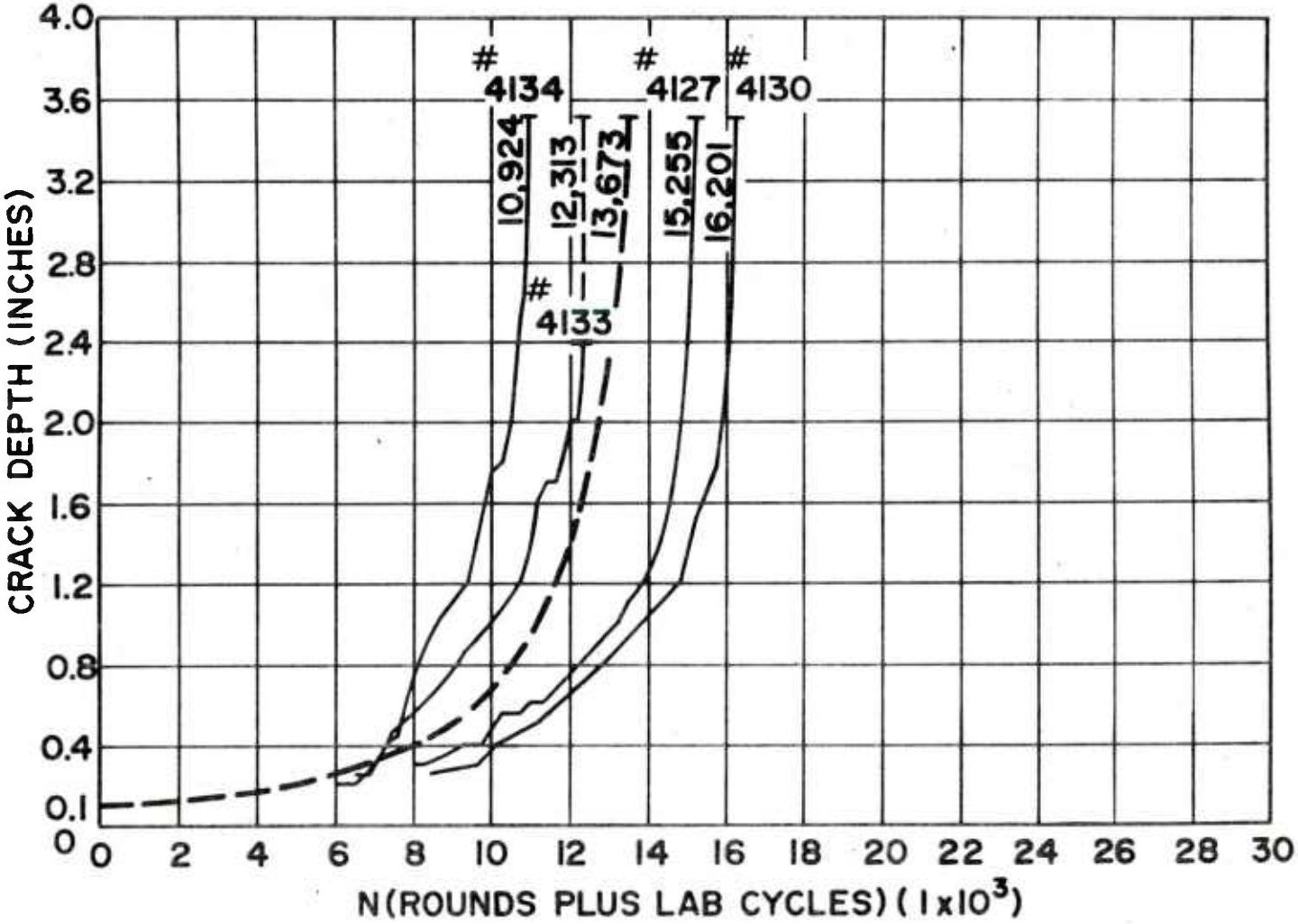

Figure 10. Crack Depth versus N, cycles, Rifled 175mm tubes. The graph shows crack depth versus fired rounds plus lab cycles from tests of four rifled 175mm tubes, showing data and a calculated representative curve to the average fatigue life from an initial crack depth of 0.10 inch.

theoretical curve shown as a dashed line. This was calculated using the values $\alpha = 0.77$, $b_i = 0.1$ inch, $B = 3.575$ inch in Equations 10, 11 and 12. This gives 6033 cycles to go from 0.10 inch to 0.25 inch depth where the first cracks were detected, and a remaining life of 7,640 cycles from there to failure, a total of 13,673 cycles. The average life of the four tubes is 13,673 cycles. These tubes were tested at the pressure of 46 ksi. The spread in life from 10,924 to 16,201 rounds-plus-cycles can be attributed to the differences in crack initiation and crack shape among the sample of four tubes. It appears that their average fatigue crack growth is approximated well by the calculated curve.

A graph of the measured crack propagation rates and the calculated rate is shown on Figure 11 for the crack depths from 0.1 inch to failure. As before, the calculated crack rates from 10^{-4} to 10^{-3} inch per cycle provide a satisfactory approximation of the measured fatigue crack growth shown on Figure 10.

A second example involves a pair of 105mm howitzer barrels[11] which were fired to failure using rounds with a pressure of 42 ksi. These barrels had a wall thickness of 1.32 inches and a diameter ratio of 1.63. They were autofrettaged to 100% overstrain, that is yielding from the bore completely to the outer surface. They had adequate properties and gave "leak-before-fracture" type failures, which were anticipated by ultrasonic monitoring of the crack depth. Figure 12

---

11. Brown, B. B., Reiner, A. N. and Davidson, T. E., "The Fatigue Life Characteristics of the 105mm M137A1 Howitzer Barrel", Watervliet Arsenal Technical Report WVT-7202, Jan. 1972

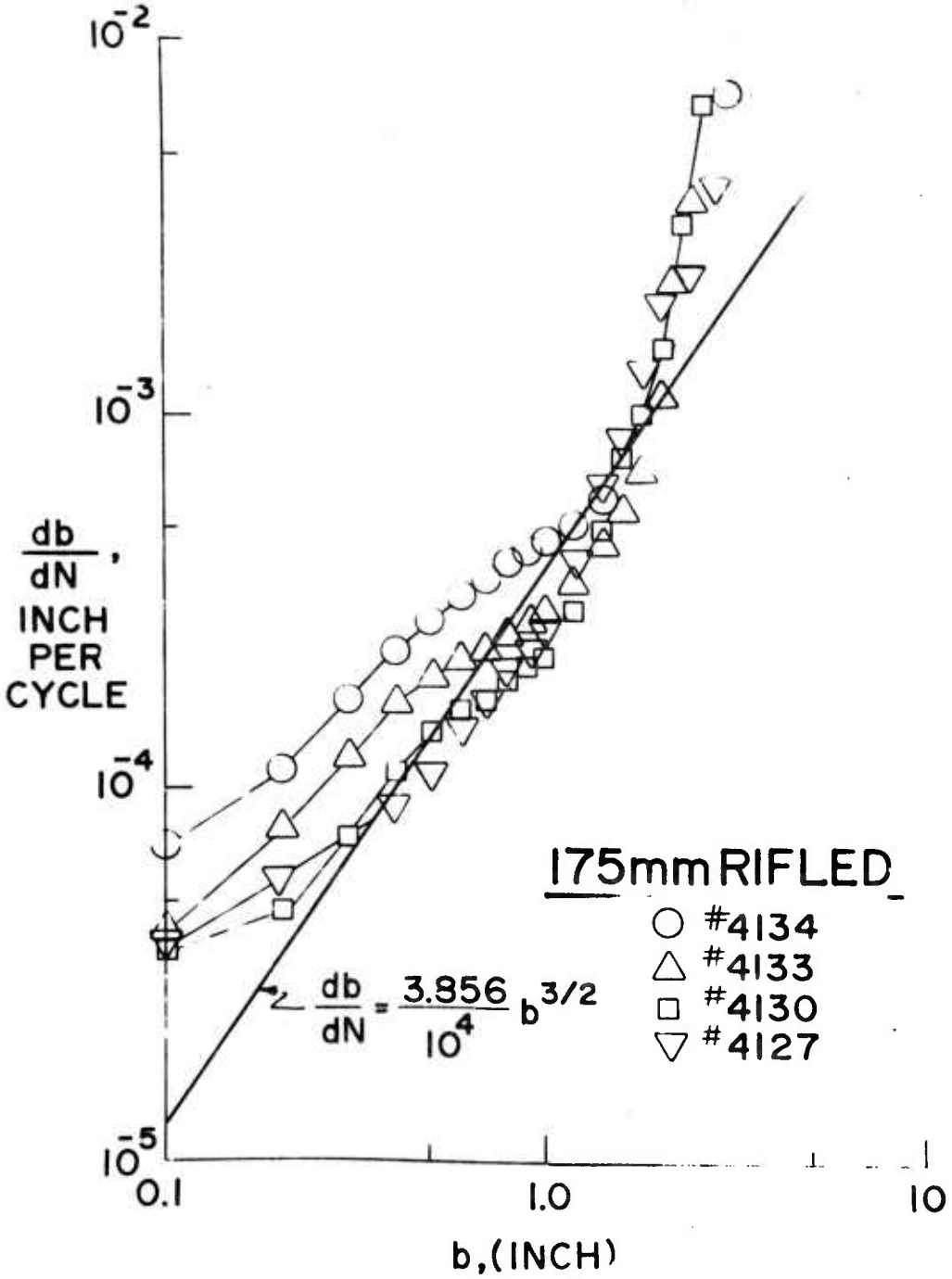

Figure 11. Crack rate versus crack depth, Rifled 175mm tubes. The log-log graph shows fatigue crack propagation rate db/dN for four rifled partially overstrained autofrettaged cannon tubes, showing data and calculated line.

shows the fracture of one of them which was intentionally produced by continuing to fire it after the fatigue crack had pierced the wall. The continued firing caused the through-crack to grow lengthwise until it became unstable and split the tube. High speed movies, taken each round for several rounds before fracture, showed the progressive enlargement of the opening. A fracture toughness of about 140 ksi $\sqrt{in}$ is required to sustain a crack of this depth.

The curves on Figure 13 show the fatigue crack growth measured by ultrasonics and a calculated curve shown as a dashed line. This was calculated using the values $\alpha = 0.832$, $b_i = 0.02$ inch and $b_f = 1.32$ inches in Equation 10, giving a life of 14,336 cycles equal to the average round life of the two tubes. The spread from 12091 to 16582 rounds may be attributed to differences in crack initiation under firing conditions.

The crack propagation rates shown in Figure 14 indicate that approximation between 5×10^{-5} inches per cycle and 5×10^{-4} inches per cycle, in this case, is sufficient to adequately approximate the fatigue crack growth curve shown on Figure 13.

The practical implication is that adequate fracture toughness and sufficient overstrain in a thinner tube produces satisfactory performance under severe service conditions.

The values of $\mathfrak{D}$ from Equation 17 for fatigue crack propagation from 0.07 B to full wall thickness B are compared with the values for the three crack shapes in the 175mm non-autofrettaged cylinder specimens in Table IV. In the 175mm tubes this is from 0.25 inch depth to 3.575 inches, while in the 105mm tubes it is from 0.09 inch to 1.32 inches.

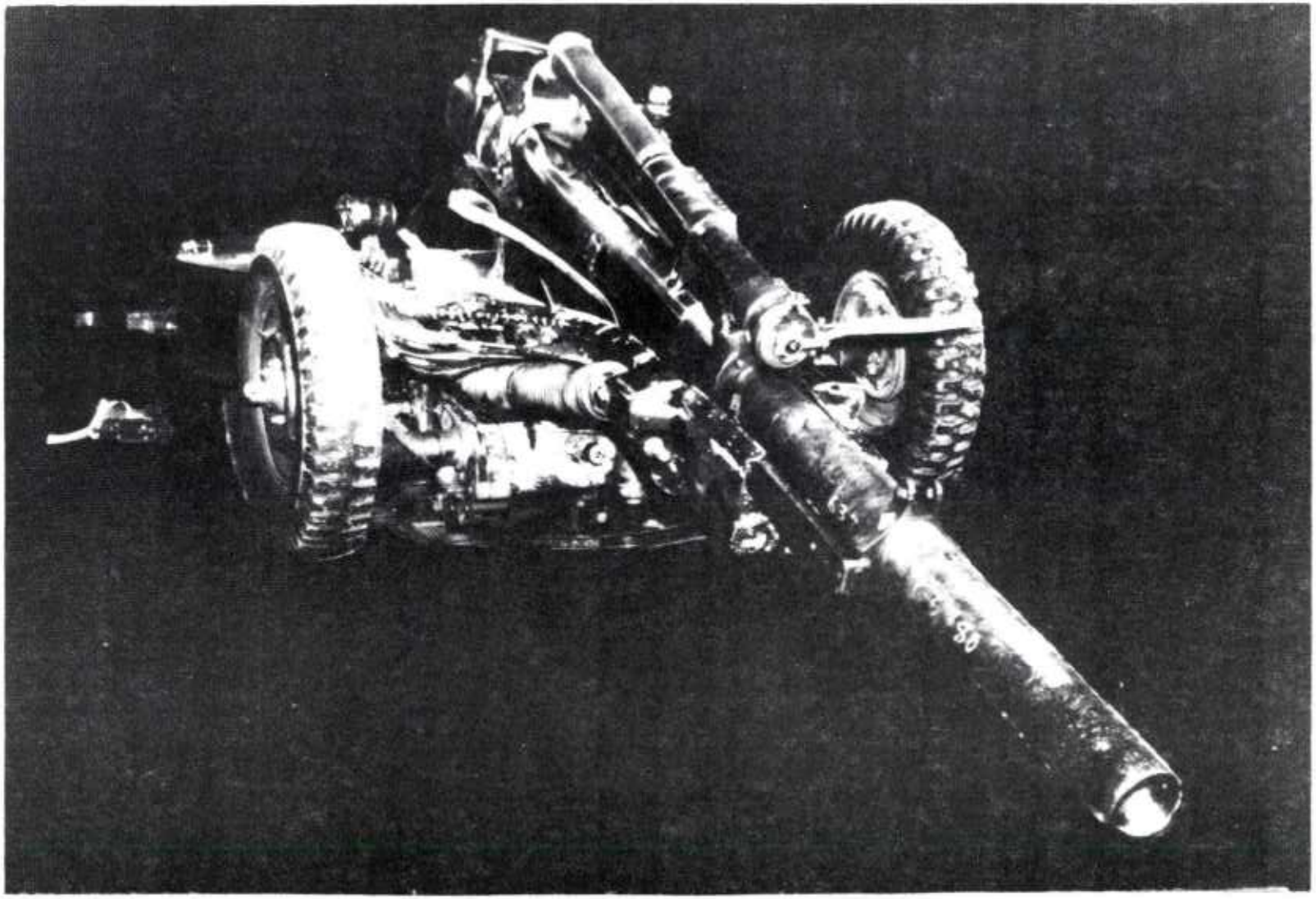

Figure 12. Fatigue failure in howitzer tube. The photo shows the fracture produced by fatigue crack growth during firing to failure of a 100% overstrained autofrettaged 105mm howitzer barrel.

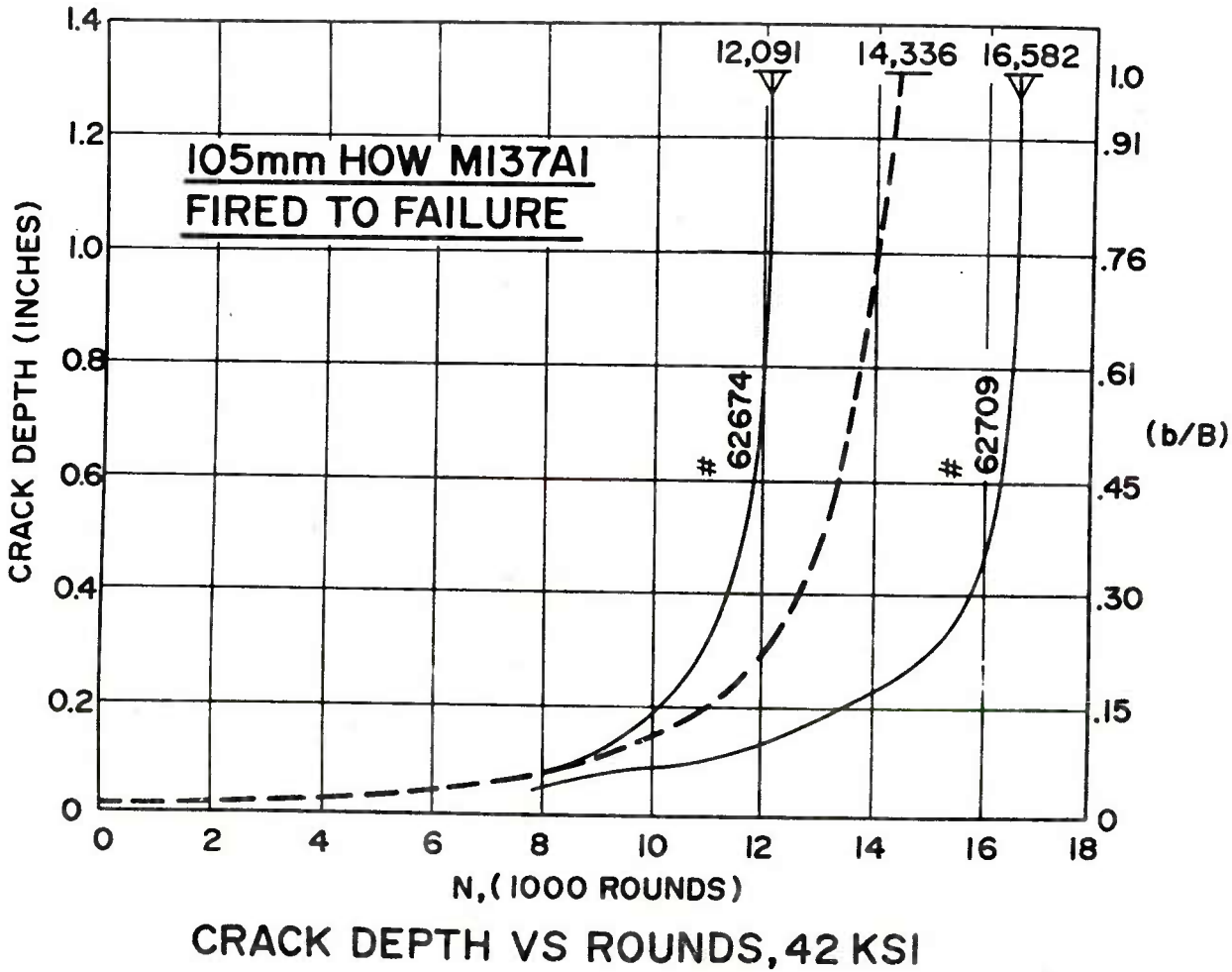

CRACK DEPTH VS ROUNDS, 42 KSI

Figure 13. Crack Depth versus N, 105mm Howitzer tube. The graph shows crack depth versus rounds fired at 42 ksi in two 105mm barrels showing data and calculated representative curve to average fatigue life from initial crack depth of 0.02 inch.

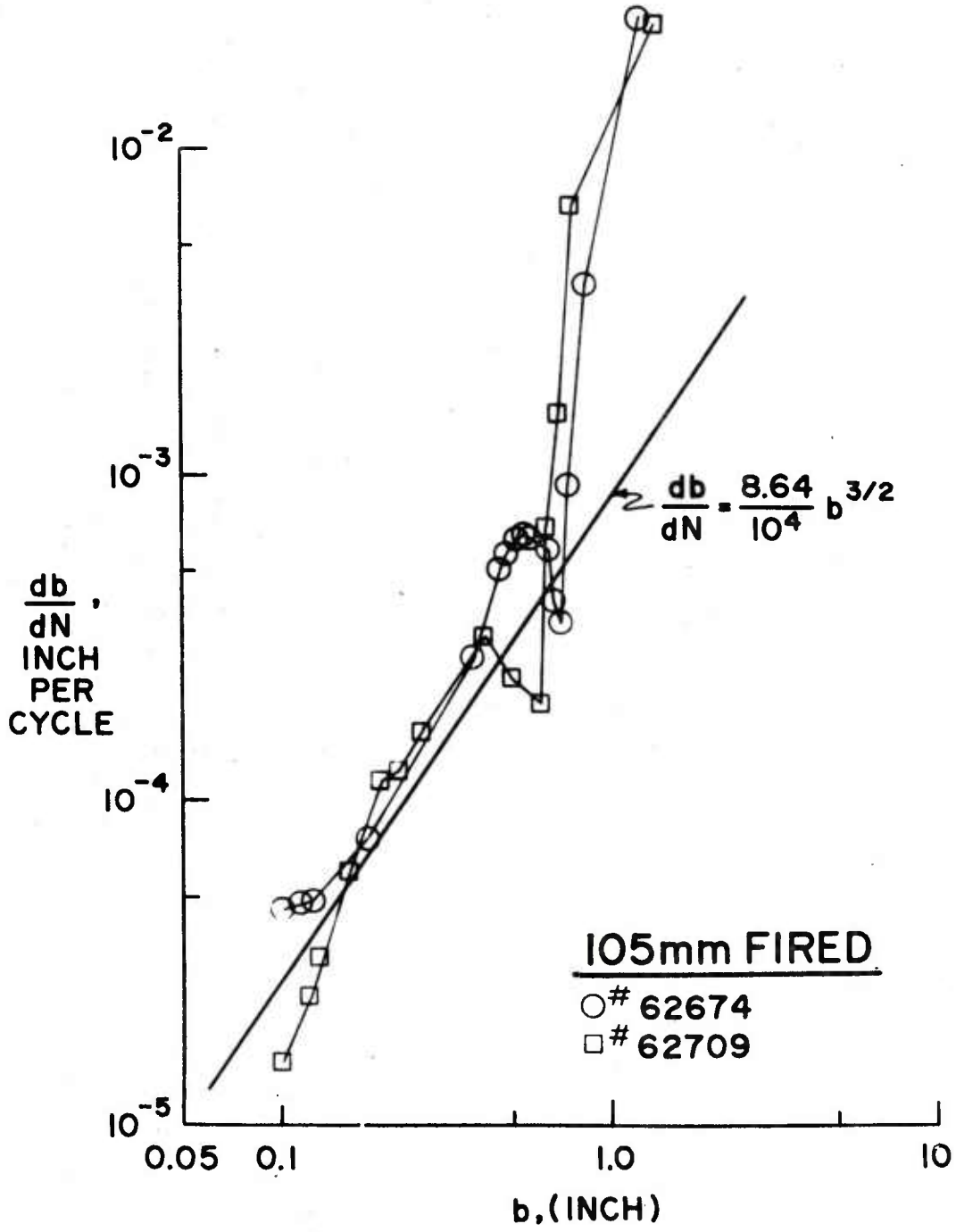

Figure 14. Crack rate versus crack depth, 105mm Howitzer tubes. The log-log graph shows fatigue crack propagation rate db/dN in two rifled 105mm fully autofrettaged howitzer barrels, showing data and calculated line.

The ratio of $\mathfrak{D}$ to that for the semicircular crack in the non-autofrettaged cylinder shows their relative fatigue crack propagation life. This ratio indicates that, on the average, both the autofrettaged 175mm tubes and the autofrettaged 105mm tubes are equivalent to a non-autofrettaged 175mm cylinder with a crack shape less severe than the 4-inch notch but more severe than the semicircle. This represents a considerable design improvement over the fatigue test results from non-autofrettaged cannon tubes. For any given configuration, the greater the percentage overstrain the larger will be the compressive residual bore stresses, which provides larger enhancement of fatigue life.

While the 105mm tubes were 100% overstrained and the 175mm tubes were only 40% overstrained, their compressive residual bore stresses were comparable because the residual stresses are a function of the percent overstrain, the diameter ratio and the yield strength. Hence at comparable pressures their fatigue performance should be about equal, as suggested by their values of $\mathfrak{D}$ in Table IV.

A plot of the values of $(N_f - N_i)$ versus $\mathfrak{D}$ from Table IV is shown on Figure 15 for all of the examples discussed, along with the line $(N_f - N_i) = 2.78\,\mathfrak{D}$. This relationship comes from Equation 16 for the ratio b_i/b_f equal to 0.07. Test results that plot below the line indicate tubes in which the α for crack shape was more severe than average or which failed early because of insufficient toughness for the crack to grow clear through the wall. Since fatigue life may be limited by fracture at less than the wall thickness in such cases, Equation 15 must also be considered in evaluating the performance.

TABLE IV

TUBE SIZES, $\mathcal{D}$, AND FATIGUE LIFE

$$\mathcal{D} = \frac{2M}{\pi^{3/2}\ \alpha^3 \left(\frac{w^2 + 1}{w^2 - 1} p\right)^3\ \sqrt{B}}$$

Tube Size & Crack Shape	P (ksi)	α	$\mathcal{D}$	$\left(\frac{\mathcal{D}}{\mathcal{D}_o}\right)$ *	N_f	N_i **	Average $(N_f - N_i)$	Cycle Ratio ***
175mm Long Curved Crack	48	1.1	825	.22	1500	0	1500	.14
175mm Semi-elliptical	48	0.954	1264	.33	3430	0	3430	.32
105mm Rifled; Fired	42 42	0.832	2012	.53	12091 16582	8300 9550	5412	.51
175mm Rifl; Fired & Cycled	46 46 46 46	0.769	2746	.72	10924 12313 15255 16201	6700 6200 7500 8400	6473	.61
175mm Semicircular	48	0.660	3819	1.0	10617	0	10617	1.0

Note: * D_o = 3819 for semicircular notch, 175mm.

** $N_i = N_{0.25"}$ for 175mm and $N_i = N_{0.092"}$ for 105mm

*** Cycle Ratio = $(N_f - N_i)/10617$

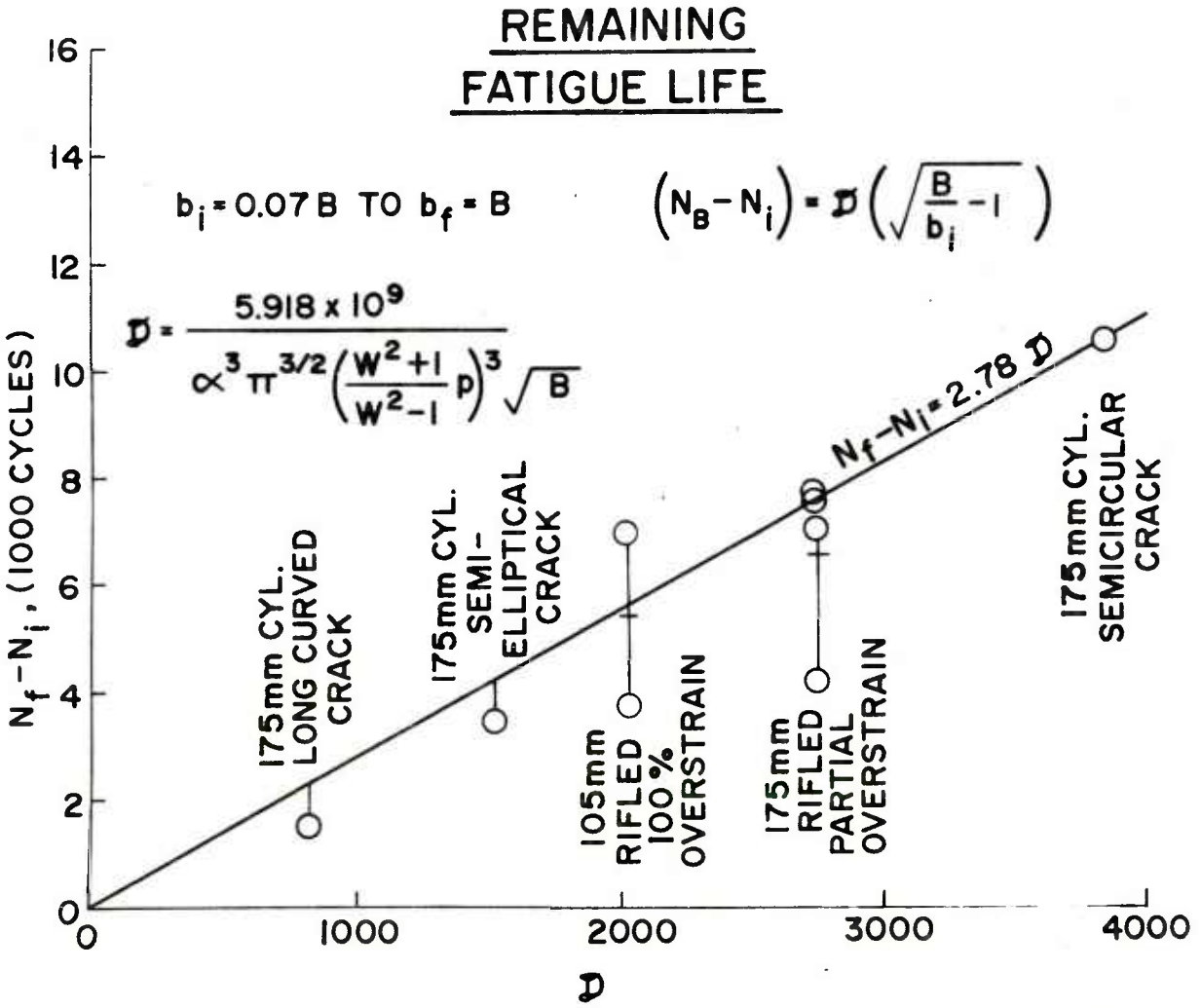

Figure 15. $(N_f - N_i)$ versus $\mathcal{D}$. The graph shows the remaining fatigue crack life versus the similitude parameter, $\mathcal{D}$, showing data from the cited examples and a calculated linear relationship for fatigue crack propagation from an initial relative crack depth of 0.07 to the final relative crack depth of 1.0 in thick walled cylinders.

The position of the points representing the average performance of the 105mm and the 175mm autofrettaged tubes on Figure 15 indicates that their behavior was nearer that of the semi-elliptical crack shape than that of the semicircular crack. This is to be expected since they were rifled tubes, which in the non-autofrettaged condition would have behaved more like the cylinder specimen with the long curved crack.

The relationships for stress intensity factors in autofrettaged cylinders are now under study. The residual stress field for partial overstrain is less and different than that for 100% overstrain. The interaction of the active stress field with the residual stress field while the crack is propagating through them is not yet well analyzed, but it is recognized that the progress of the crack must permit the residual stresses to relax and equilibrate ahead of the crack front. Experimental evaluation of similar pre-notched autofrettaged cylinder specimens is in progress and will be reported later.

In the meantime, until more precise expressions become available, these concepts and idealizations of fracture mechanics and fatigue crack propagation can provide the rationale for calculating fatigue lives and estimating the effects of different design variables upon the fatigue and fracture of thick-walled cylinders. They also point the way toward obtaining more valid equations in the future.

CONCLUSIONS

1. The fatigue crack propagation rates for part-through wall cracks in thick-walled cylinders can be approximated by the product of a materials constant times the cube of the stress intensity factor range.

2. The stress intensity factor expression $K = Y S\sqrt{\pi b}$ can be approximated by $K = \alpha S \sqrt{\pi b}$, wherein the variable Y is replaced by a constant α which depends upon the crack shape and the stress state.

3. The upper bound of K is expressed by the Bowie and Freese equation which is for a straight fronted notch. For non-autofrettaged cylinders of 2.0 diameter ratio this is approximated by $K = 1.79 S \sqrt{\pi b}$, where S is the tangential bore stress. The lower bound corresponds to a semicircular crack shape and is expressed by $K = 0.66 S \sqrt{\pi b}$.

4. At any measureable crack depth, b, the remaining fatigue life for "leak-before-fracture" may be estimated by $(N_f - N_i) = \mathfrak{D}\left[\sqrt{\frac{B}{b}} - 1\right]$ where $\mathfrak{D}$ depends upon design variables. Adequate toughness must be provided to prevent fracture at crack depths less than the wall thickness.

5. Design variables such as materials properties, operating pressure, diameter ratio, wall thickness and residual stresses determine the stress intensity factor, which in turn controls the fatigue crack propagation rate and the failure crack depth. These design variables may be adjusted to optimize the fatigue life expectancy and to avoid brittle fracture.

ACKNOWLEDGEMENTS

This work was performed under funding from Project Number 1T162105AH84 of the Army Materials and Mechanics Research Center, Watertown, Mass.

Our sincere gratitude goes to Robert R. Fujczak for data analysis, Ronald T. Abbott for fatigue testing, David P. Kendall and J. M. Delaney for help in autofrettage, Abraham Rubin and John Zalinka for ultrasonic measurements, John Genthner for photographic records, Bruce Brown and his staff for assistance in testing and Joan Peterson for typing.

REFERENCES

1. Paris, P. C. "The Fracture Mechanics Approach to Fatigue", in Fatigue, an Interdisciplinary Approach, Burke, J. J., Reed, N. L., Weiss, V., Editors, Syracuse University Press (1964) pp 107-132.

2. Paris, P. C. and Sih, G. C. "Stress Analysis of Cracks" in Fracture Toughness Testing and Its Applications ASTM-STP 381, Am. Soc. for Testing and Mats. (1965) pp 38-40.

3. Timoshenko, S. and Goodier, J. N. "Theory of Elasticity", McGraw Hill Book Co., N. Y., Third Edition, p 71.

4. Bowie, O. L. and Freese, C. E., "Elastic Analysis for A Radial Crack in a Circular Ring", Engineering Fracture Mechanics, (1972) Vol. 4, pp 315-321.

5. Underwood, J. H., Lasselle, R. R., Scanlon, R. D. and Hussain, M. A., A Compliance K-Calibration for a Pressurized Thick-Wall Cylinder With A Radial Crack", Engineering Fracture Mechanics, (1972) Vol. 4, pp 231-244.

6. Smith, C. W., Jolles, M. and Hu, T., "Stress Intensities For Low Aspect Ratio Surface Flaws in Pressurized Thick Walled Tubes", Virginia Poly. Inst. Report VPI-E-75-19, Aug. 1975, Blacksburg, VA. 24061.

7. Hussain, M. A., Pu, S. L., Scanlon, R. D., and Throop, J. F., "Stress Intensity Factor for A Pressurized Thick-wall Cylinder with Part Through Circular Flaw, Collocation Method and Compliance Calibration", in preparation, (1976).

8. Barsom, J. M., "The Dependence of Fatigue Crack Propagation on Strain Energy Release Rate and Crack Opening Displacement", in Damage Tolerance in Aircraft Structures", ASTM-STP 486, Am. Soc. for Testing and Mats. (1971) pp 1-15.

9. Throop, J. F. and Miller, G. A., "Optimum Fatigue Crack Resistance", in "Achievement of High Fatigue Resistance in Metals and Alloys", ASTM-STP 467, Am Soc. for Testing and Mats. (1970), pp 154-168.

10. Davidson, T. E., Reiner, A. N., Brown, B. B., Throop, J. F., Miller, J. J. and Austin, B. A., "The Fatigue Life Characteristics of the 175mm M113E1 Gun Tube", Watervliet Arsenal Technical Report WVT-6912, March 1969.

11. Brown, B. B., Reiner, A. N. and Davidson, T. E., "The Fatigue Life Characteristics of the 105mm M137A1 Howitzer Barrel", Watervliet Arsenal Technical Report WVT-7202, Jan. 1972.

WATERVLIET ARSENAL INTERNAL DISTRIBUTION LIST

May 1976

	No. of Copies
COMMANDER	1
DIRECTOR, BENET WEAPONS LABORATORY	1
DIRECTOR, DEVELOPMENT ENGINEERING DIRECTORATE	1
ATTN: RD-AT	1
RD-MR	1
RD-PE	1
RD-RM	1
RD-SE	1
RD-SP	1
DIRECTOR, ENGINEERING SUPPORT DIRECTORATE	1
DIRECTOR, RESEARCH DIRECTORATE	2
ATTN: RR-AM	1
RR-C	1
RR-ME	1
RR-PS	1
TECHNICAL LIBRARY	5
TECHNICAL PUBLICATIONS & EDITING BRANCH	2
DIRECTOR, OPERATIONS DIRECTORATE	1
DIRECTOR, PROCUREMENT DIRECTORATE	1
DIRECTOR, PRODUCT ASSURANCE DIRECTORATE	1
PATENT ADVISORS	1

EXTERNAL DISTRIBUTION LIST

December 1976

1 copy to each

OFC OF THE DIR. OF DEFENSE R&E
ATTN: ASST DIRECTOR MATERIALS
THE PENTAGON
WASHINGTON, D.C. 20315

CDR
US ARMY TANK-AUTMV COMD
ATTN: AMDTA-UL
AMSTA-RKM MAT LAB
WARREN, MICHIGAN 48090

CDR
PICATINNY ARSENAL
ATTN: SARPA-TS-S
SARPA-VP3 (PLASTICS
TECH EVAL CEN)
DOVER, NJ 07801

CDR
FRANKFORD ARSENAL
ATTN: SARFA
PHILADELPHIA, PA 19137

DIRECTOR
US ARMY BALLISTIC RSCH LABS
ATTN: AMXBR-LB
ABERDEEN PROVING GROUND
MARYLAND 21005

CDR
US ARMY RSCH OFC (DURHAM)
BOX CM, DUKE STATION
ATTN: RDRD-IPL
DURHAM, NC 27706

CDR
WEST POINT MIL ACADEMY
ATTN: CHMN, MECH ENGR DEPT
WEST POINT, NY 10996

CDR
HQ, US ARMY AVN SCH
ATTN: OFC OF THE LIBRARIAN
FT RUCKER, ALABAMA 36362

CDR
US ARMY ARMT COMD
ATTN: AMSAR-PPW-IR
AMSAR-RD
AMSAR-RDG
ROCK ISLAND, IL 61201

CDR
US ARMY ARMT COMD
FLD SVC DIV
ARMCOM ARMT SYS OFC
ATTN: AMSAR-ASF
ROCK ISLAND, IL 61201

CDR
US ARMY ELCT COMD
FT MONMOUTH, NJ 07703

CDR
REDSTONE ARSENAL
ATTN: AMSMI-RRS
AMSMI-RSM
ALABAMA 35809

CDR
ROCK ISLAND ARSENAL
ATTN: SARRI-RDD
ROCK ISLAND, IL 61202

CDR
US ARMY FGN SCIENCE & TECH CEN
ATTN: AMXST-SD
220 7TH STREET N.E.
CHARLOTTESVILLE, VA 22901

DIRECTOR
US ARMY PDN EQ. AGENCY
ATTN: AMXPE-MT
ROCK ISLAND, IL 61201

EXTERNAL DISTRIBUTION LIST (Cont)

1 copy to each

CDR
US NAVAL WPNS LAB
CHIEF, MAT SCIENCE DIV
ATTN: MR. D. MALYEVAC
DAHLGREN, VA 22448

DIRECTOR
NAVAL RSCH LAB
ATTN: DIR. MECH DIV
WASHINGTON, D.C. 20375

DIRECTOR
NAVAL RSCH LAB
CODE 26-27 (DOCU LIB.)
WASHINGTON, D.C. 20375

NASA SCIENTIFIC & TECH INFO FAC
PO BOX 8757, ATTN: ACQ BR
BALTIMORE/WASHINGTON INTL AIRPORT
MARYLAND 21240

DEFENSE METALS INFO CEN
BATTELLE INSTITUTE
505 KING AVE
COLUMBUS, OHIO 43201

MANUEL E. PRADO / G. STISSER
LAWRENCE LIVERMORE LAB
PO BOX 808
LIVERMORE, CA 94550

DR. ROBERT QUATTRONE
CHIEF, MAT BR
US ARMY R&S GROUP, EUR
BOX 65, FPO N.Y. 09510

2 copies to each

CDR
US ARMY MOB EQUIP RSCH & DEV COMD
ATTN: TECH DOCU CEN
FT BELVOIR, VA 22060

CDR
US ARMY MAT RSCH AGCY
ATTN: AMXMR - TECH INFO CEN
WATERTOWN, MASS 02172

CDR
WRIGHT-PATTERSON AFB
ATTN: AFML/MXA
OHIO 45433

CDR
REDSTONE ARSENAL
ATTN: DOCU & TECH INFO BR
ALABAMA 35809

12 copies

CDR
DEFENSE DOCU CEN
ATTN: DDC-TCA
CAMERON STATION
ALEXANDRIA, VA 22314

NOTE: PLEASE NOTIFY CDR, WATERVLIET ARSENAL, ATTN: SARWV-RT-TP, WATERVLIET, N.Y. 12189, IF ANY CHANGE IS REQUIRED TO THE ABOVE.